International Journal of Minerals, Metallurgy and Materials
Volume 30, Number 11, November 2023, Page 2191
https://doi.org/10.1007/s12613-023-2660-3

Waste heat recovery from hot steel slag on the production line: Numerical simulation, validation and industrial test

Tianhua Zhang[1,2], *Longheng Xiao*[1], *Guibo Qiu*[2], *Huigang Wang*[2]✉, *Min Guo*[1], *Xiangtao Huo*[1], *and Mei Zhang*[1]✉

1) State Key Laboratory of Advanced Metallurgy, School of Metallurgical and Ecological Engineering, University of Science and Technology Beijing, Beijing 100083, China

2) Central Research Institute of Building and Construction Co., Ltd., MCC Group, Beijing 100088, China

(Received: 18 January 2023; revised: 21 April 2023; accepted: 21 April 2023)

Abstract: Waste heat recovery from hot steel slag was determined in a granular bed through the combination of numerical simulation and an industrial test method. First, the effective thermal conductivity of the granular bed was calculated. Then, the unsteady-state model was used to simulate the heat recovery under three different flow fields (O-type, S-type, and nonshielding type (Nontype)). Second, the simulation results were validated by *in-situ* industrial experiments. The two methods confirmed that the heat recovery efficiencies of the flow fields from high to low followed the order of Nontype, S-type, and O-type. Finally, heat recovery was carried out under the Nontype flow field in an industrial test. The heat recovery efficiency increased from ~76% and ~78% to ~81% when the steel slag thickness decreased from 400 and 300 to 200 mm, corresponding to reductions in the steel slag mass from 3.96 and 2.97 to 1.98 t with a blower air volume of 14687 m^3/h. Therefore, the research results showed that numerical simulation can not only guide experiments on waste heat recovery but also optimize the flow field. Most importantly, the method proposed in this paper has achieved higher waste heat recovery from hot steel slag in industrial scale.

Keywords: hot steel slag; calculation and verification; industrial tests; waste heat recovery

1. Introduction

A large amount of energy is consumed during iron and steel smelting, which has become the key industry contributing to carbon emissions. China's National Bureau of Statistics states that more than half of the crude steel in the world was produced in China (approximately 1033 million tons in 2021). The steel industry produced approximately 18% of the national carbon emissions. Reducing CO_2 emissions is strongly required to prevent global warming. Under these circumstances, China proposed the strategic goal of "emission peak and carbon neutrality" in an attempt to develop technologies for reducing CO_2 emissions. The residual heat of steel slag is a promising heat energy resource that can be recovered. Generally, the temperature of steel slag in the molten state is higher than 1400°C, and the calorific value of the residual heat in steel slag is higher than that of other types of residual heat [1–3]. The released heat could reach 1.6 GJ when 1 t steel slag drops from 1400°C to room temperature [4–5]. This amount of released heat is almost equal to the heat released by burning 50–60 kg of standard coal. However, the current steel slag treatment technology could not realize heat recovery on an industrial scale, resulting in the considerable waste of more than five million tons of standard coal per year. As a result, the corresponding increase in CO_2 emissions reached approximately 13 million tons. Hence, heat recovery is crucial for carbon emission reduction.

The existing treatment technologies for steel slag (including atmospheric hot stuffy self-disintegration, pressured hot stuffy self-disintegration, high-pressure water steam, and atmospheric aging processes) mainly focus on the separation and utilization of slag and iron [6–11]. Although some heat recovery methods for steel slag, including the air quenching method, roller method, and methane reforming reaction, have been conducted previously, they are limited to laboratory research, and most attempts at their industrialization have failed. These processes require good slag fluidity, which depends on high temperature and stable chemical compositions [2,12–16]. However, the steel slag temperature always drops rapidly, and the chemical compositions of steel slag are prone to fluctuation, resulting in poor slag fluidity. Therefore, developing a suitable heat recovery method for any physical state, namely solid, semisolid, and liquid, on the industrial scale is urgently needed.

Granular beds are widely used as heat-transfer devices in the chemical field, metallurgy, and other fields. Normally, heat transfer between particles involves conduction, convec-

✉ Corresponding authors: Mei Zhang E-mail: zhangmei@ustb.edu.cn; Huigang Wang E-mail: wanghuigang0822@126.com

tion, and radiation [17]. In addition to heat transfer between contacting or adjacent particles, radiative heat transfer occurs between noncontact particles [18–20]. This type of transfer becomes increasingly important with the increase in temperature. Particularly, when the temperature exceeds 800°C, radiative heat transfer between noncontact particles becomes the dominant mode of heat transfer. Numerical simulation has become an important way to study heat transfer in high-temperature granular beds for reducing experimental blindness. By using computational fluid dynamics (CFD), Wang *et al.* [21] investigated forced convection heat transfer in a granular bed. Abdulmohsin and Al-Dahhan [22] researched the effect of cooling gas flow rate and bed structure on the convective heat transfer coefficient by using an experimental device with a diameter of 0.3 m and experimental methods. By using DEM–CFD coupling simulation and treating the filler as a porous medium, Sharma *et al.* [23] explored the heat-transfer characteristics in a rectangular bed reactor filled with spherical particles. Moreover, they compared the heat-transfer characteristics predicted by porous media treatment and DEM–CFD coupling methods. Their results showed that the simulation calculation had high reliability when spherical particles were taken as a porous medium.

In our previous work, we performed the industrial test of heat recovery from hot steel slag under the O-type flow field of granular beds [24]. In this work, we proposed S-type and nonshielding type (Nontype) flow fields and explored their effects on waste heat recovery from steel slag to identify the optimal flow field type. To reduce blindness and optimize the flow field for waste heat recovery, numerical simulation was first used to predict the efficiency of waste heat recovery under three different flow fields on the basis of the calculation of the valid thermal conductivity and effective view factor. Subsequently, an industrial test was conducted to verify the simulation results. Finally, heat recovery on the assembly line was carried out under the optimal flow field. This work may provide a new idea for mutual verification between numerical simulations and industrial tests to improve the success rate of industrial tests and finally realize an industrial breakthrough in heat recovery from hot steel slags.

2. Heat recovery procedure

The image of steel slag heat recovery is shown in Fig. 1 (a). Accordingly, the chain grate machine was a cuboid with a length of 3.0 m, a width of 1.5 m, and a height of 1.0 m. Cooling air was blown from the bottom of the chain grate and collected by the pipeline of the gas fume after passing through the hot steel slag. In this work, three flow fields of the air inlet at the bottom of the chain grate, namely, O-type, S-type, and Nontype, were designed (Fig. 1(b)–(d)). Their actual physical pictures are given in Fig. 1(e)–(g). The thermocouples located at A and B in Fig. 1(a) were used to measure the temperature of the steel slag and hot gas fume, respectively. The distance between the thermocouples located at A and the cooling air inlet plane was 100 mm. The steel slag temperature data were the thermocouple measurements. Similarly, the temperature of high-temperature air was the measured values of the thermocouples located at B. Meanwhile, gas flowmeters were also installed at B to measure the flow of the hot gas fume. During the experiments, steel slag with a temperature of (1150 ± 20)°C (particle size ≤100 mm)

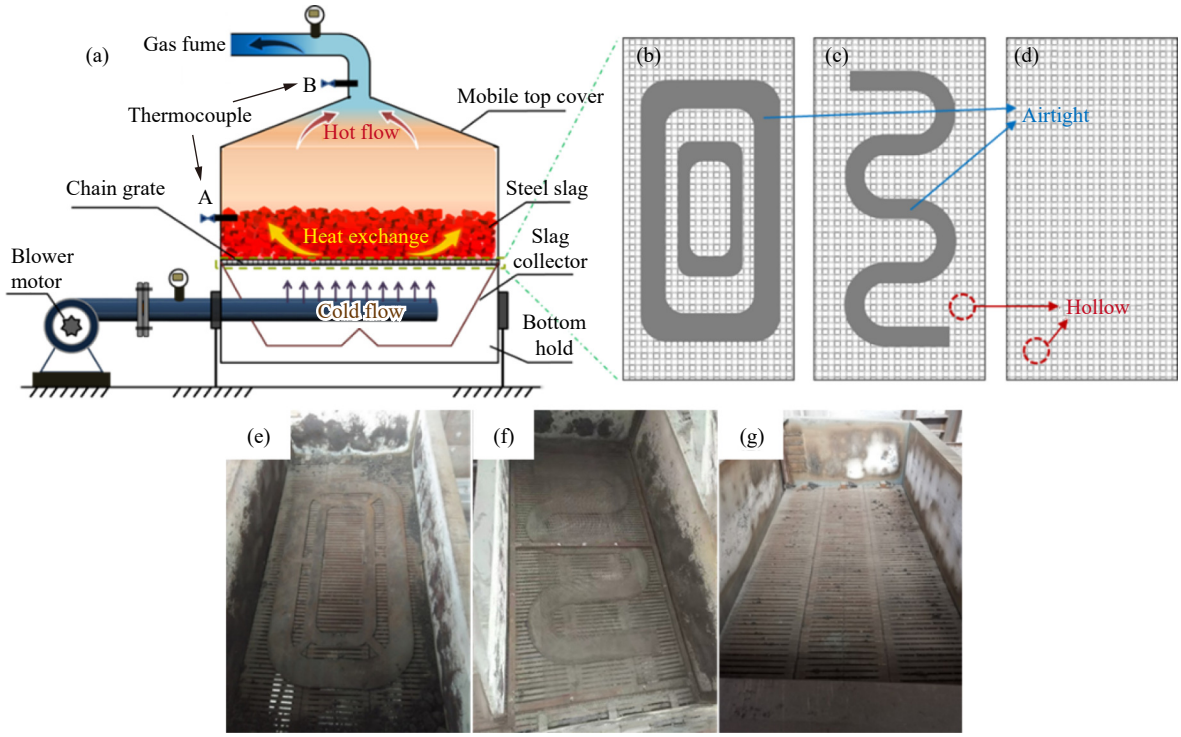

Fig. 1. (a) Schematic of heat recovery from hot steel slag, different flow field diagrams of (b) O-type, (c) S-type, and (d) Nontype, and corresponding physical pictures of (e) O-type, (f) S-type, and (g) Nontype with a length of 3.0 m, a width of 1.5 m, and a height of 1.0 m.

was placed in a chain gate machine and then separately piled up to thicknesses of 200, 300, 400, and 500 mm (the corresponding steel slag mass is 1.98, 2.97, 3.96 and 4.95 t). Next, the cooling air entered from the bottom of the chain grate to exchange heat with the hot steel slag. The blower air volumes were 7866, 14687, 20075, and 26500 m^3/h, respectively. Heat recovery from steel slag could be calculated in accordance with the hot air flow volume, the temperature at location B, and other data.

3. Model establishment and numerical simulation

In an effort to reduce blindness and optimize the flow field of waste heat recovery, the numerical simulation based on the established model was first used to predict the waste heat recovery under the three different flow fields.

3.1. Model establishment

3.1.1. Effective thermal conductivity of granular beds.

As we already described in the introduction section, heat transfer includes convection, conduction, and heat radiation. Radiative heat transfer would become the dominant mode when the material temperature exceeds 800°C. In addition, the effective view factor and valid thermal conductivity of the granular bed when the steel slag temperature reaches 1150°C would be two important parameters for calculating gas–solid heat transfer in the bed. In our previous work, the empirical formula for the effective view factors of a binary-sized granular bed with a random distribution was obtained by fitting the Monte Carlo method calculation results. The corrected formula of effective radiation thermal conductivity can be referred in our previous paper [25], which is helpful for the calculation of heat transfer.

3.1.2. Basic assumptions.

We proposed the following assumptions to simplify the simulation of steel slag cooling in a granular bed (chain grate machine): (1) The chemical reaction between cooling air and steel slag was not considered. (2) The contact thermal resistance between steel slag particles was not considered. (3) Air was an ideal incompressible gas. (4) The characteristics of isotropic heat transfer for steel slag particles were the same, with an initial temperature of 1150°C and uniform distribution. (5) The thickness of the chain grate was not considered.

3.1.3. Basic equations

In the calculation of the heat transfer of hot steel slag and air in the granular bed, the steel slag particles were regarded as a whole porous medium. Specifically, the heat transfer between steel slag particles and air in the granular bed was simulated by using a porous medium model. The simulation test was conducted in accordance with the actual heat exchange conditions, and the mathematical model is shown in Fig. 2. The length and width of the model were 3 and 1.5 m, respectively. The height dimension (z-axis direction) was the steel slag's thickness, and the cooling air entered from $z = 0$ and flowed along the positive z-axis direction. The flow

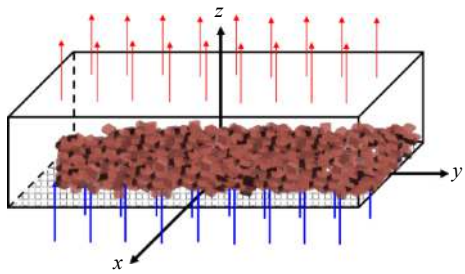

Fig. 2. Geometric model of waste heat recovery from steel slag.

fields of the air inlet were O-type, S-type, and Nontype, as indicated in Fig. 1.

Heat transfer occurred between slag particles and air when cooling air entered the granular bed. The air was in a turbulent flow state when it passed through the porous medium, and the steel slag temperature decreased with time. Therefore, the unsteady-state model was adopted to solve the simulation. The heat transfer in steel slag cooling conformed to the air flow control formula.

(1) Mass conservation formula.

$$\frac{\partial \rho}{\partial t} + \frac{\partial (\rho u)}{\partial x} + \frac{\partial (\rho v)}{\partial y} + \frac{\partial (\rho w)}{\partial z} = 0 \tag{1}$$

(2) Momentum conservation formula.

The x-axis direction:

$$\frac{\partial (\rho u)}{\partial t} + \nabla (\rho u \vec{v}) = \rho g_x - \frac{\partial P}{\partial x} + \mu \left(\frac{\partial^2 u}{\partial x^2} + \frac{\partial^2 u}{\partial y^2} + \frac{\partial^2 u}{\partial x^2 z} \right) \tag{2}$$

The y-axis direction:

$$\frac{\partial (\rho v)}{\partial t} + \nabla (\rho v \vec{v}) = \rho g_y - \frac{\partial P}{\partial y} + \mu \left(\frac{\partial^2 v}{\partial x^2} + \frac{\partial^2 v}{\partial y^2} + \frac{\partial^2 v}{\partial x^2 z} \right) \tag{3}$$

The z-axis direction:

$$\frac{\partial (\rho w)}{\partial t} + \nabla (\rho w \vec{v}) = \rho g_z - \frac{\partial P}{\partial z} + \mu \left(\frac{\partial^2 w}{\partial x^2} + \frac{\partial^2 w}{\partial y^2} + \frac{\partial^2 w}{\partial x^2 z} \right) \tag{4}$$

(3) Energy conservation formula.

$$\frac{\partial}{\partial t}(\rho T) + \frac{\partial}{\partial x_i}(\rho \vec{v} T) = \frac{k}{c_p} \frac{\partial^2 T}{\partial x_i \partial x_j} + S_T \tag{5}$$

In Eq. (1) to (5), ρ is the air density, g·cm^{-3}; t represents time, s; u, v, and w represent the velocity components in the x-axis, y-axis, and z-axis, respectively, m·s^{-1}; $\vec{v}$ is the air velocity, m·s^{-1}; P represents the pressure, Pa; g_m represents the gravitational acceleration component in the direction of each coordinate axis ($m = x, y, z$), m·s^{-2}; T represents the air temperature, K; μ is the viscosity coefficient; k represents the thermal conductivity, W·m^{-1}·K^{-1}; c_p is the air's specific heat capacity, kJ·kg^{-1}·K^{-1}; x_i and x_j are coordinate positions (i, j = 1, 2, and 3, representing the x, y, and z directions, respectively), m; S_T is the entropy value of air at temperature T, J·mol^{-1}·K^{-1}.

3.1.4. Heat transfer model

The steel slag in the granular bed was regarded as a whole porous material. Therefore, in this work, the porous medium model in the ANSYS Fluent software was used for the numerical simulation of heat exchange. The model can be used

to simulate working conditions with complex geometry, fine pores, and large size differences but cannot be solved by grid division. The simulation method for the porous media model regarded the solid phase in the flow region as the resistance applied to the fluid. Furthermore, the resistance effect, such as gas penetration through the particle accumulation bed, was considered. Therefore, the model was very suitable for the experimental process of this work.

The different geometric lengths (such as the size of pores) and physical properties of steel slag and cooling air (i.e., the temperature difference between the porous skeleton and fluid) could lead to the local temperature difference between these two phases. Therefore, the nonequilibrium model in the ANSYS Fluent software was adopted.

3.1.5. Boundary conditions

The working conditions of waste heat recovery from steel slag under three flow fields are exhibited in Table 1, and the heat-transfer simulation was performed on the basis of these data. The initial temperature (25°C) and flow rate of air at the inlet could be set by CFD in Fluent Software. The simulated outlet was a free boundary condition, and the air flowed out under the action of pressure.

3.2. Numerical simulation of steel slag heat recovery

In accordance with the description given in Section 2, the flow field of the air inlet under the O-type was relatively complex such that the air flow velocity and temperature change may be relatively complex in steel slag heat recovery. To clarify the air velocity and temperature change during heat exchange, the variation in the velocities and temperatures of cooling air with position and time were simulated under an O-type flow field.

Table 1. Working conditions of waste heat recovery from steel slag under three flow fields

Experiment conditions	O-type	S-type	Nontype
Blower air volume / ($m^3 \cdot h^{-1}$)	14687	14687	14687
Steel slag thickness / mm	400	400	400
Steel slag mass / t	3.96	3.96	3.96
Area of air passing through the bottom of the chain grate / m^2	3.01	3.27	4.50

3.2.1. Process simulation under the O-type flow field

The cloud diagram of cooling air velocity at different planes along the z-axis in the O-type flow field is shown in Fig. 3. The Fig. 3(a) illustrates that the velocity of air at the bottom (z = 0) hollow part (red area) was large and then gradually decreased when air passed through the slag at z = 200 mm (Fig. 3(b)) and z = 400 mm (Fig. 3(c)). However, the velocity of air passing the O-type baffle at z = 0 plane was basically 0 (blue area), so that the steel slag located on the baffle cannot adequately undergo convective heat exchange with air. Fig. 3(c) depicts that the air velocity became more uniform when it passed through the porous area. Specifically, the velocity above the O-type baffle gradually increased and that in the hollow part gradually decreased. Meanwhile, the results also indicated that the overall air velocity along the z-axis was reduced due to blockage by the O-type baffle and steel slag particles.

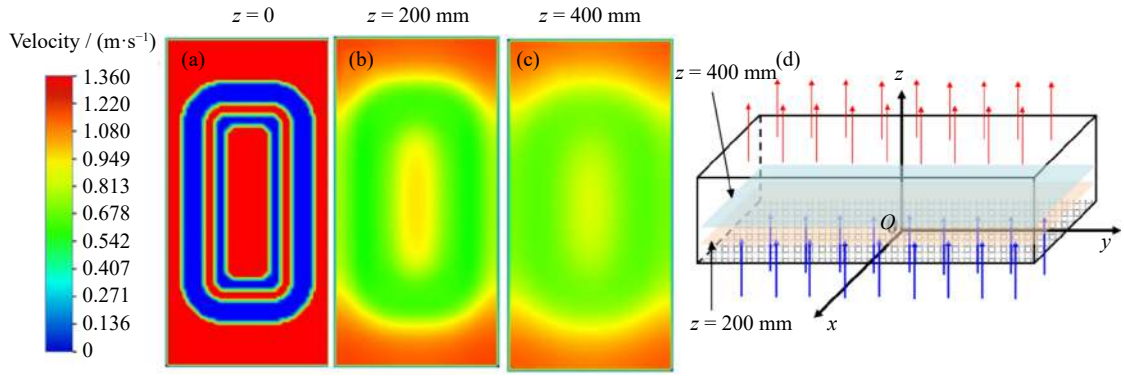

Fig. 3. Cloud diagram of cooling air velocity at different planes along the z-axis at 5400 s: (a) z = 0; (b) z = 200 mm; (c) z = 400 mm. (d) Plane position diagram of z = 200 mm and 400 mm.

Fig. 4 shows the vector diagram of cooling air velocity in cross-section x = 0 at 5400 s. The air speed decreased greatly and flowed along the y-axis direction after the air entered the bed due to the barrier imposed by the baffle. Then, the flow velocity in the porous region (steel slag) gradually became uniform and only flowed along the z-axis direction, which took a greater role in the heat transfer of steel slag. This result was consistent with the finding shown in Fig. 3.

Fig. 5 shows the variation in the temperatures of steel slag and air along the line of the y-axis (x = 0, z = 0, −1.5 m < y < 1.5 m) at 5400 s. Clearly, the temperature distribution of steel slag had the same trend as that of the air. These trends were symmetrically distributed with y = 0 as the center. The peak value of the temperature plot in Fig. 5 corresponded to the position of the O-type baffle. This characteristic could be attributed to the low air flow velocity and insufficient heat exchange with steel slag at the baffle, which resulted in a low cooling speed and a high temperature of the steel slag. Similarly, because of the low air flow velocity, less air was available for heat exchange with the steel slag at the same time period, thus resulting in higher air temperature. Therefore, the baffle would hinder heat transport between air and slag. That is, the effect of heat transport between air and slag on the upper part of the baffle was insufficient.

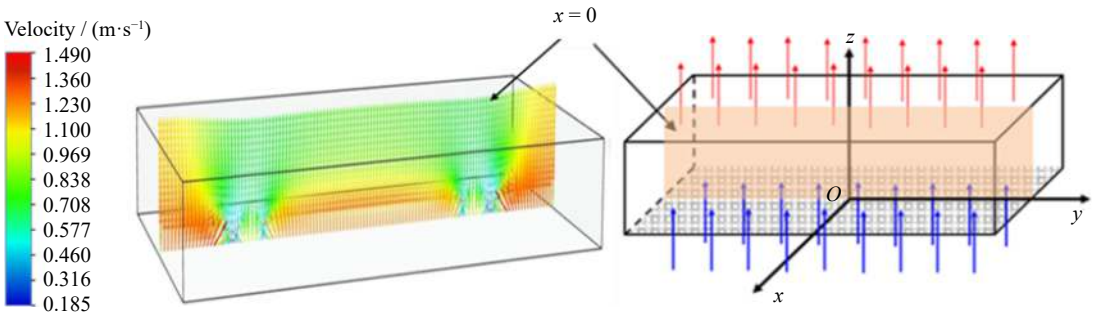

Fig. 4. Vector diagram of cooling air velocity in section $x = 0$ at 5400 s.

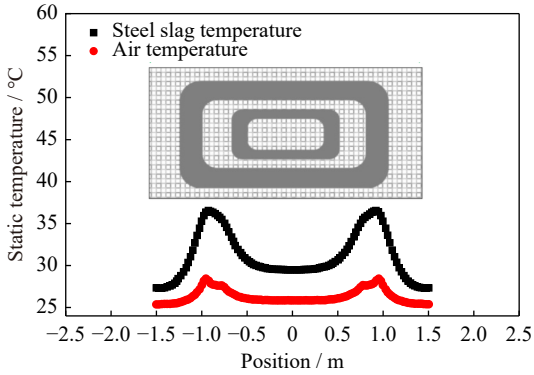

Fig. 5. Temperature variation of the steel slag and air along the y-axis ($x = 0$, $z = 0$, -1.5 m $< y <$ 1.5 m) at 5400 s.

3.2.2. Simulation of the effect of different flow fields on waste heat recovery

To investigate the effect of flow fields on slag heat recovery, the change in air temperature during steel slag cooling under the O-type, S-type, and Nontype flow fields was first simulated (Fig. 6). The air temperature was the highest at the beginning of the calculation. With the prolongation of heat exchange time, the heat of the steel slag was gradually removed by the air, thus reducing the temperature of the steel slag. Therefore, the air temperature also decreased gradually. Fig. 6 shows that the maximum air temperature under the three different flow fields differed. The highest temperature values were approximately 450, 410, and 370°C under the Nontype, S-type, and O-type flow fields, respectively.

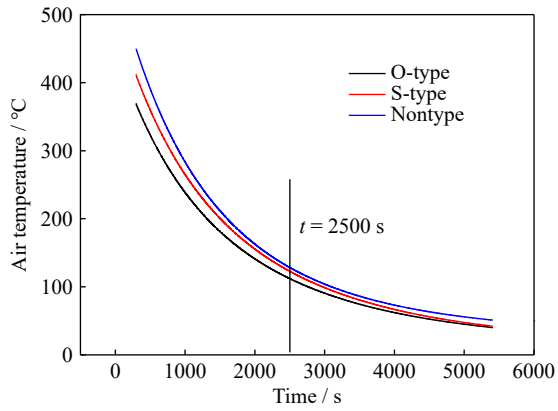

Fig. 6. Calculation results of air temperature as a function of time under different flow fields (the blower air volume was 14687 m³/h, and the slag had a thickness of 400 mm and a mass of 3.96 t).

Moreover, under the same experimental time conditions, the air temperature under the Nontype flow field was always the highest, whereas that under the O-type flow field was always the lowest. In accordance with the simulation calculation results presented in Section 3.2.1, the baffle at the air inlet of the chain grate bottom will affect the heat exchange between the steel slag and air. Table 1 shows that the inlet area of the O-type flow field yielded the smallest value of only 3.01 m². This result, in turn, indicated that the shielding area was the largest. Therefore, given that the steel slag on the baffle could not fully exchange heat with the cooling air under the same blower air volume, the smaller the shielding area, the more heat transport between the cooling air and steel slag, and then the higher the temperature. Finally, the air temperature under the Nontype flow field was the highest under the same experimental conditions.

In addition, the heat exchange process could be divided into two stages in accordance with the rate of the decline in air temperature, as shown in Fig. 6: the front stage of the former 2500 s and the rear stage of the latter 2900 s. The decline rate of air temperature was high in the front stage and was highest under the Nontype flow field. In the rear stage, the rate of decline gradually flattened. At the end of the calculation, the air temperature under the three flow fields became very close within a range of 30–50°C. Generally, in the early stage, the temperature difference between the steel slag and air was large such that the obtained heat of the air was considerably higher under the same flow and time, and the cooling of the steel slag was rapid, thus resulting in the larger rate of decline in air temperature. However, in the later stage, the temperature difference became small, and the cooling of the steel slag also decelerated. Therefore, the rate of decline in the cooling air temperature was reduced accordingly.

The heat absorbed by cooling air is proportional to the integral of the temperature curve from 0 to 5400 s. Therefore, under the Nontype flow field, the heat absorbed by air was the largest, and the corresponding heat recovery efficiency should also be the highest. The absorbed heat was the smallest under the O-type flow field. Therefore, the corresponding heat recovery efficiency should also be the lowest. The heat recovery efficiencies under different flow fields were calculated in accordance with Eqs. (6)–(8), and the results are shown in Fig. 7.

$$Q_t = c_a m_a (T_t - T_{a0}) = c_a \rho_a V_a \mathrm{d}t (f(t) - T_{a0}) \quad (6)$$

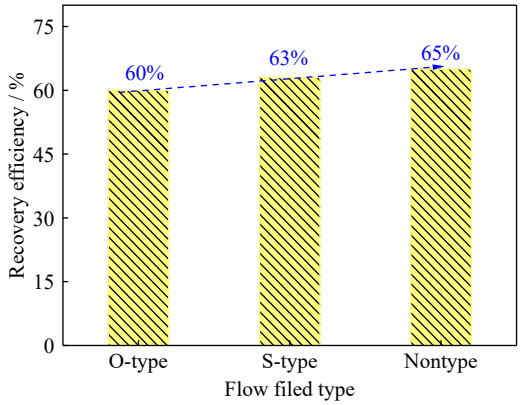

Fig. 7. Calculation results of heat recovery efficiency under different flow fields (the blower air volume was 14687 m^3/h, and the slag had a thickness of 400 mm and a mass of 3.96 t).

$$Q_a = \int_0^t Q_t \mathrm{d}t = \int_0^t (c_a \rho_a V_a f(t) - c_a \rho_a V_a T_0)\mathrm{d}t = \int_0^t (c_a \rho_a V_a f(t)\mathrm{d}t - c_a \rho_a V_a T_0 \mathrm{d}t) = \int_0^t c_a \rho_a V_a f(t)\mathrm{d}t - \int_0^t c_a \rho_a V_a T_0 \mathrm{d}t \quad (7)$$

$$\eta = \frac{Q_a}{Q_{st}} \times 100\% \quad (8)$$

where Q_t is the recovered heat with the experiment proceeding to t s, kJ; c_a represents the air specific heat capacity at the average temperature, kJ/(kg·°C); t represents the experimental procedure time, s; T_t ($f(t)$) is the air temperature's time tested under point B at t s, °C; m_a represents the mass of air, kg; ρ_a represents the density of air at the average temperature, kg/m^3; V_a represents the average air flow determined at point B, m^3/h; T_{a0} is the room temperature, i.e., 25°C; Q_a represents the heat consumed by air throughout the experiment, kJ; and Q_{st} is the released total heat of the slag during the temperature change from 1150 to 25°C, kJ.

The heat recovery efficiency was clearly the highest under the Nontype flow field and, consistent with the previous analysis, was the lowest under the O-type flow field. The recovery efficiencies were approximately 65%, 63% and 60% under the Nontype, S-type, and O-type flow fields, respectively.

4. Validation of the simulation and the industrial test

4.1. Industrial validation of the numerical simulation of heat recovery under different flow fields

The calculation results in Section 3.2.2 showed that the air temperature and heat recovery efficiency of the Nontype flow field were the largest. To verify the feasibility of the calculation results in actual production, industrial experiments on steel slag heat recovery were carried out under three different flow fields at a blower air volume of 14687 m^3/h and slag thickness of 400 mm. As shown in Fig. 8(a), the air temperature under different flow fields first increased rapidly to their maximum values and then decreased slowly. Moreover, similar to the calculation results, the air temperature under the Nontype flow field was always the highest during the whole experimental process. This phenomenon was related to the sufficient heat exchange between air and steel slag. However, the experimental results of the O-type and S-type flow fields were slightly different from the calculated results. From the beginning to 1600 s of the process, the air temperature under the O-type flow field was larger than that under the S-type flow field. After 1600 s, the air temperature under the S-type flow field was larger than that under the O-type flow field, the same as the calculation results. Fig. 8(a) shows that the air temperature under the S-type flow field was abnormal; that is, it suddenly decreased then suddenly increased when the experiment lasted for approximately 200 s, likely due to the sudden increase in air volume caused by the vibration of the equipment or the instability of the blower air volume. The above reasons might also account for the lower air temperature of the S-type flow field than that of the O-type flow field in the first 1600 s of the experiment. In addition, similar to that depicted in Fig. 6, the air temperature could also be divided into two stages. Namely, the rate of temperature decline was large in the first 2500 s and gradually flattened in the later 2900 s of the experiment.

Subsequently, the efficiency of steel slag heat recovery under the three flow fields was calculated, and the results are given in Fig. 8(b). The heat recovery experiments under the Nontype flow field had the highest heat efficiency of approx-

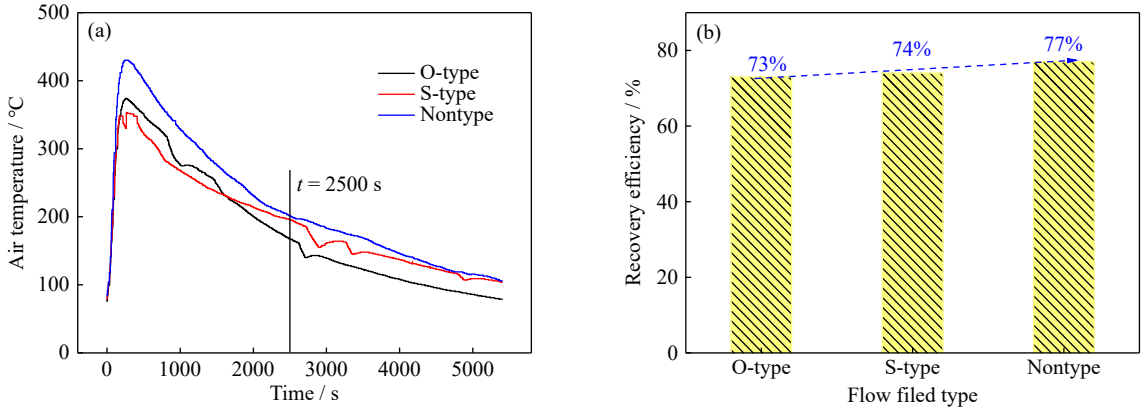

Fig. 8. (a) Variation in air temperature as a function of time and (b) efficiency of heat recovery under different flow fields (the blower air volume was 14687 m^3/h, and the slag had a thickness of 400 mm and a mass of 3.96 t).

imately 77%. However, the heat recovery experiments under the O-type flow field had the lowest heat efficiency of approximately 73%. The above results conformed to the above calculation results (Section 3.2.2); that is, the heat recovery efficiency from high to low followed the order of Nontype, S-type, and O-type. Therefore, the simulation calculation used in this study can well guide engineering practice.

4.2. Industrial test of heat recovery from hot steel slag under the Nontype flow field

To realize the breakthrough in heat recovery from steel slag, an industrial test under the optimal flow field (Nontype) was carried out, as described in the following section.

4.2.1. Effect of blower air volume

The air temperature at different blower air volumes is depicted in Fig. 9(a). Notably, the steel slag thickness was 400 mm, which corresponded to a mass of 3.9 t. Fig. 9(a) clearly shows that the air temperature increased rapidly at first, then decreased sharply, and finally became almost unchanged. The initial increase in temperature can be attributed to the hysteresis in thermocouple temperature measurement. In addition, the maximum temperature of air differed at different blower air volumes. Specifically, the maximum air temperature could reach ~480°C at an air volume of 7866 m^3/h but was only ~380°C at an air volume of 26500 m^3/h, likely because the total heat obtained by the air certainly originated from the same amount of hot steel slag. Hence, with the increase in blower air volume, the amount of air used to cool the steel slag increased. The air temperature decreased with the increase in air volume. In addition, the temperature decline rate can be divided into two stages, with a higher decline rate in the first 2500 s stage. Meanwhile, an obvious phenomenon could be observed from Fig. 9(a): The air temperature at lower blower air volumes was always higher than that at larger air flows in the stable stage (after ~1000 s). This phenomenon would continue until the end of the experiment. The heat released by the 3.96 t steel slag during cooling from 1150°C to room temperature could be determined on the basis of the heat calculation formula of $Q = cm(T_{si} - T_{s0})$ (where Q is released heat of steel slag, kJ; c is the specific heat capacity of steel slag, kJ/(kg·°C); m is the mass of steel slag, kg; T_{si} is the initial temperature of steel slag before waste heat recovery, 1150°C; T_{s0} is room temperature, 25°C). In short, under the same test conditions, the smaller the air flow used to cool the steel slag, the less the heat removed from the steel slag within the same time, and the more the rest heat of the steel slag. This characteristic resulted in the high air temperature at low blower air volumes.

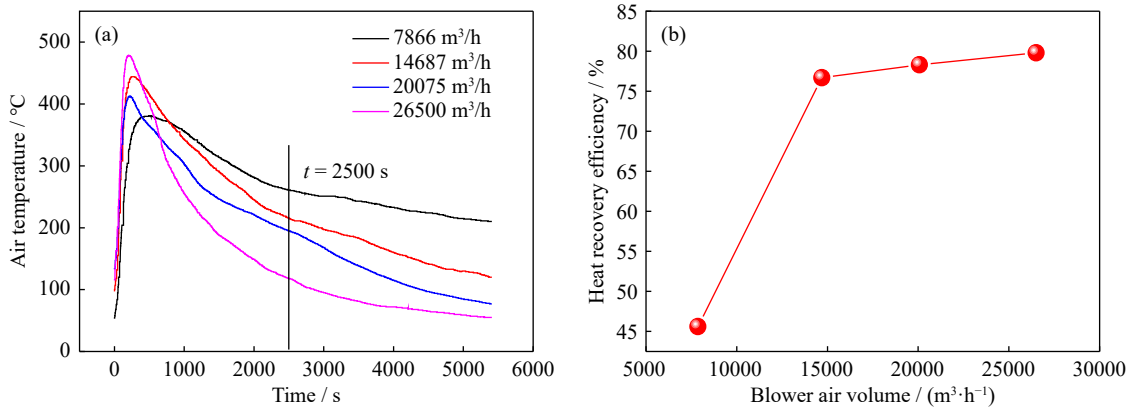

Fig. 9. (a) Variation in temperature as a function of time and (b) recovery efficiency of heat at different blower air volumes (the slag has a thickness of 400 mm and a mass of 3.96 t).

The heat recovery efficiency is exhibited in Fig. 9(b). Accordingly, the value of heat recovery efficiency first increased, then plateaued with the increase in blower air volume, demonstrating that the blower air volume had an important influence on the efficiency of heat recovery from hot steel slag. Specifically, the increase in blower air volume from 7866 to 14687 m^3/h resulted in a steep increase in heat recovery efficiency from ~45% to ~77%. Then, with the further increase in air volume to 26500 m^3/h, the heat recovery efficiency was maintained at ~79%. Under the same heat exchange time, the obtained heat of the cooling air increased when the air flow increased. Therefore, more heat in the steel slag was removed within the same test time, resulting in a low slag temperature. Meanwhile, the radiant heat loss of low-temperature steel slag was smaller. The above reasons led to high heat recovery efficiency with large air flow.

The purpose of this work is to realize effective heat recovery. The relationship between heat recovery efficiency and blower air volume should also be taken into account. Therefore, the optimal blower air volume was set to 14687 m^3/h.

4.2.2. Effect of the thickness of the hot steel slag

As illustrated in Fig. 10(a), we also investigated the changes in air temperature at different steel slag thicknesses (200, 300, 400, and 500 mm, corresponding to 1.98, 2.97, 3.96, and 4.95 t in mass, respectively) and a blower air volume of 14687 m^3/h. Similar to the results shown in Fig. 9(a), the air temperature also increased rapidly in the initial stage and decreased slowly after reaching its maximum value. Within ~260 s, the temperature reached its maximum values of ~345, ~409, ~443, and ~453°C at the steel slag thicknesses of 200, 300, 400, and 500 mm, respectively. As described in Section 4.2.1, air temperatures increased rapidly in the initial stage of the experiment due to the hysteresis caused by thermocouple measurement. Fig. 10(a) also illus-

trates that the decline rate of air temperature differed at different times due to the difference between the slag and air temperatures. In addition, the air temperature started to decrease after ~260 s, and its decline rate increased when the steel slag thickness decreased. Specifically, when the experiment was performed for 2500 s, the air temperatures decreased from their maximum values to ~260, ~215, ~170 and ~130°C at the different steel slag thicknesses of 500, 400, 300, and 200 mm, respectively. At the end of the test (5400 s), the air temperatures were ~200, ~120, ~88, and ~55°C.

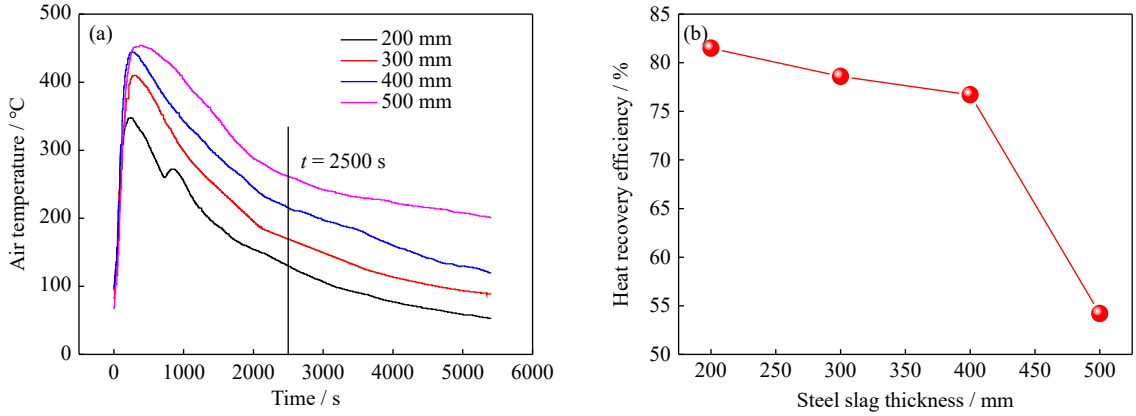

Fig. 10. (a) Variation in temperature as a function of time and (b) changes in heat recovery efficiency with different slag thicknesses (the blower air volume was 14687 m^3/h).

As shown in Fig. 10(b), the heat recovery efficiency decreased from ~81% and ~78% to ~76% when the steel slag thickness was increased from 200 and 300 to 400 mm. When the slag thickness increased to 500 mm, the recovery efficiency decreased sharply to ~54%. Under the same air flow rate, the amount of air (equivalent unit slag mass) increased with the decrease in slag amount. Hence, at the same blower air volume, the cooling speed of the steel slag was rapid when the thickness of the steel slag was smaller (i.e., a smaller mass of steel slag), resulting in higher heat recovery. Meanwhile, with the reduction in time, the heat transport between the slag and the surrounding environment decreased, thus reducing heat loss. Finally, on the basis of the above factors, the value of heat recovery efficiency reached the maximum when the slag thickness was 200 mm. When the thickness was increased to 300, 400, and 500 mm, the amount of air required for cooling the steel slag decreased, which extended the cooling time. Additionally, with the increase in the steel slag thickness, the air resistance increased, leading to an increase in air loss, i.e., a reduction in air flow through point B (Fig. 11), ultimately leading to a reduction in the efficiency of waste heat recovery from the steel slag.

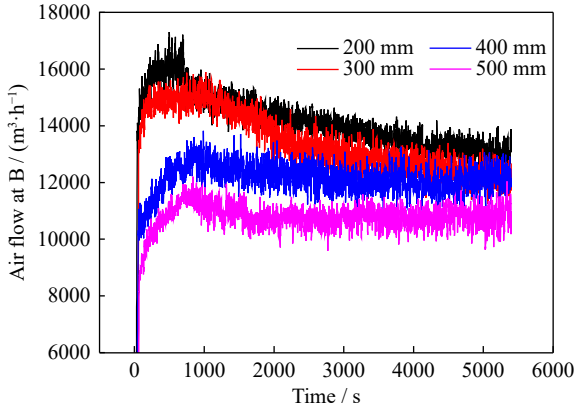

Fig. 11. Real-time air flow volume detested at location B with different thicknesses of steel slag (blower air volume: 14687 m^3/h).

Existing reports show that the efficiency of heat recovery from slag is between 40% and 75% [14,26–28]. The efficiency in this work reached 77%–79%. First, through numerical simulation, we identified the flow field of the granular bed that was most conducive to waste heat recovery from steel slag. Second, the heat exchange granular bed was well sealed in the experimental process. This condition also contributed to heat recovery from steel slag. Therefore, the waste heat recovery efficiency obtained in this work was higher than that reported in the literature.

5. Conclusions

Heat recovery from hot steel slag in a granular bed was conducted through a combination of simulation calculations and industrial tests. Under the industrial test conditions, the steel slag particles in the granular bed were regarded as a whole porous media, and heat transport between the slag and cooling air was simulated by using an unsteady-state model in Fluent Software. The simulation results showed that the baffle of the air inlet hindered heat transport between the air and slag, conferring the steel slag and air with a higher temperature than the region where air can pass directly. The simulation and experimental results confirmed that under the same experimental conditions, the heat recovery efficiency of the Nontype flow field was the highest, followed by that of the S-type and O-type flow fields. The results of the industrial tests demonstrated that the blower air volume and the steel slag thickness (mass) had important effects on heat recovery. At the same steel slag thickness of 400 mm, the heat recovery efficiency increased from ~45% to ~79% with the increase in the blower air volume from 7866 to 26500 m^3/h. At the same blower air volume, the heat recovery efficiency increased from ~54% to ~81% with a decrease in steel slag

thickness from 500 to 200 mm (mass from 4.95 to 1.98 t). In summary, the research results reported in this paper showed that numerical simulations can optimize the flow field and guide the industrial test of heat recovery from steel slag. Moreover, an industrial breakthrough in high-efficiency heat recovery from steel slag was achieved.

Acknowledgements

This work was financially supported by the National Natural Science Foundation of China (No. 51972019) and the National Key Research and Development Program of China (No. 2019YFC1905702).

Conflict of Interest

Mei Zhang is an editorial board member for this journal and was not involved in the editorial review or the decision to publish this article. The authors declare that they have no known competing financial interests or personal relationships that could have appeared to influence the work reported in this paper.

References

[1] H. Matsuura, X. Yang, G. Li, Z. Yuan, and F. Tsukihashi, Recycling of ironmaking and steelmaking slags in Japan and China, *Int. J. Miner. Metall. Mater.*, 29(2022), No. 4, p. 739.[PubMed].

[2] Y. Sun, S, Seetharaman, Q, Liu, Z, Zhang, L, Liu, and X. Wang, Integrated biomass gasification using the waste heat from hot slags: Control of syngas and polluting gas releases, *Energy*, 114(2016), p. 165.

[3] N. Shigaki, H. Tobo, S. Ozawa, Y. Ta, and K. Hagiwara, Heat recovery process from packed bed of hot slag plates, *ISIJ Int.*, 55(2015), No. 10, p. 2258.

[4] R.M. McDavid and B.G. Thomas, Flow and thermal behavior of the top surface flux/powder layers in continuous casting molds, *Metall. Mater. Trans. B*, 27(1996), No. 4, p. 672.

[5] Y.Q. Sun, Z.T. Zhang, L.L. Liu, and X.D. Wang, Heat recovery from high temperature slags: A review of chemical methods, *Energies*, 8(2015), No. 3, p. 1917.

[6] L. Andreas, S. Diener, and A. Lagerkvist, Steel slags in a landfill top cover - Experiences from a full-scale experiment, *Waste Manage.*, 34(2014), No. 3, p. 692.

[7] L.H. Zhao, W. Wei, H. Bai, X. Zhang, and D.Q. Cang, Synthesis of steel slag ceramics: Chemical composition and crystalline phases of raw materials, *Int. J. Miner. Metall. Mater.*, 22(2015), No. 3, p. 325.

[8] L.D. Poulikakos, C. Papadaskalopoulou, B. Hofko, *et al*., Harvesting the unexplored potential of European waste materials for road construction, *Resour. Conserv. Recycl.*, 116(2017), p. 32.

[9] M.X. Shi, Q. Wang, and Z.K. Zhou, Comparison of the properties between high-volume fly ash concrete and high-volume steel slag concrete under temperature matching curing condition, *Constr. Build. Mater.*, 98(2015), p. 649.

[10] P.E. Tsakiridis, G.D. Papadimitriou, S. Tsivilis, and C. Koroneos, Utilization of steel slag for Portland cement clinker production, *J. Hazard. Mater.*, 152(2008), No. 2, p. 805.

[11] P. Xue, A.J. Xu, D.F. He, *et al*., Research on the sintering process and characteristics of belite sulphoaluminate cement produced by BOF slag, *Constr. Build. Mater.*, 122(2016), p. 567.

[12] B. Ismail and W. Ahmed, Thermoelectric power generation using waste-heat energy as an alternative green technology, *Recent Pat. Electr. Eng.*, 2(2009), No. 1, p. 27.

[13] G. Bisio, Energy recovery from molten slag and exploitation of the recovered energy, *Energy*, 22(1997), No. 5, p. 501.

[14] H.N. Zhang, J.P. Dong, C. Wei, C.F. Cao, and Z.T. Zhang, Future trend of terminal energy conservation in steelmaking plant: Integration of molten slag heat recovery-combustible gas preparation from waste plastics and CO_2 emission reduction, *Energy*, 239(2022), art. No. 122543.

[15] W.B. Chen, M.H. Wang, L.L. Liu, H. Wang, and X.D. Wang, Three-stage method energy–mass coupling high-efficiency utilization process of high-temperature molten steel slag, *Metall. Mater. Trans. B*, 52(2021), No. 5, p. 3004.

[16] N. Maruoka, T. Mizuochi, H. Purwanto, and T. Akiyama, Feasibility study for recovering waste heat in the steelmaking industry using a chemical recuperator, *ISIJ Int.*, 44(2004), No. 2, p. 257.

[17] W. van Antwerpen, C.G. du Toit, and P.G. Rousseau, A review of correlations to model the packing structure and effective thermal conductivity in packed beds of mono-sized spherical particles, *Nucl. Eng. Des.*, 240(2010), No. 7, p. 1803.

[18] J.D. Felske, Approximate radiation shape factors between two spheres, *J. Heat Transfer*, 100(1978), No. 3, p. 547.

[19] J.R. Howell, The Monte Carlo method in radiative heat transfer, *J. Heat Transfer*, 120(1998), No. 3, p. 547.

[20] M.L. Pitso, *Characterisation of Long Range Radiation Heat Transfer in Packed Pebble Bed* [Dissertation], North-West University, Evanston, 2011, p. 68.

[21] S.C. Wang, C.Y. Xu, W. Liu, and Z.C. Liu, Numerical study on heat transfer performance in packed bed, *Energies*, 12(2019), No. 3, art. No. 414.

[22] R.S. Abdulmohsin and M.H. Al-Dahhan, Characteristics of convective heat transport in a packed pebble-bed reactor, *Nucl. Eng. Des.*, 284(2015), p. 143.

[23] A. Sharma, A. Thakur, S.K. Saha, A. Sharma, D. Sharma, and P. Chaudhuri, Thermal-hydraulic characteristics of purge gas in a rectangular packed pebble bed of a fusion reactor using DEM-CFD and porous medium analyses, *Fusion Eng. Des.*, 160(2020), art. No. 111848.

[24] T.H. Zhang, G.B. Qiu, H.G. Wang, M. Guo, F.Q. Cheng, and M. Zhang, In-suit industrial tests of the highly efficient recovery of waste heat and reutilization of the hot steel slag, *ACS Sustainable Chem. Eng.*, 9(2021), No. 10, p. 3955.

[25] T.H. Zhang, C.P. Liu, H.G. Wang, M. Guo, M. Zhang, Numerical simulation of radiative heat transfer in a binary-size granular bed, *Therm. Sci.*, 26(2022), No. 6B, p. 5095.

[26] T. Mizuochi, T. Akiyama, T. Shimada, E. Kasai, and J.I. Yagi, Feasibility of rotary cup atomizer for slag granulation, *ISIJ Int.*, 41(2001), No. 12, p. 1423.

[27] H. Zhang, H. Wang, X. Zhu, *et al*., A review of waste heat recovery technologies towards molten slag in steel industry, *Appl. Energy*, 112(2013), p. 956.

[28] Y. Zhang, J. Zhang, T.Y. Zhang, Y.M. Liu, and Z.B. Han, Analysis of steel slag treatment technology and waste heat recovery technology, *China Metall.*, 24(2014), No. 8, p. 33.